

Article

Effect of Surface Passivation on Photoelectrochemical Water Splitting Performance of WO₃ Vertical Plate-Like Films

Yahui Yang ¹, Renrui Xie ¹, Yang Liu ², Jie Li ² and Wenzhang Li ^{2,*}

¹ College of Resources and Environment, Hunan Agricultural University, Changsha 410128, China; E-Mails: Yangyahui2002@sina.com (Y.Y.); pure_xrr@hotmail.com (R.X.)

² School of Chemistry and Chemical Engineering, Central South University, Changsha 410083, China; E-Mails: yang_liu.1989@yahoo.com (Y.L.); lijieliu@csu.edu.cn (J.L.)

* Author to whom correspondence should be addressed; E-Mail: liwenzhang@csu.edu.cn; Tel./Fax: +86-731-8887-9616.

Academic Editor: Bunsho Ohtani

Received: 22 October 2015 / Accepted: 17 November 2015 / Published: 24 November 2015

Abstract: WO₃ vertical plate-like arrays provide a direct pathway for charge transport, and thus hold great potential as working electrodes for photoelectrochemical (PEC) water splitting. However, surface recombination due to surface defects hinders the performance improvement. In this work, WO₃ vertical plate-like arrays films with HfO₂ passivation layer were fabricated via a simple dip-coating method. In the images of transmission electron microscope, a fluffy layer and some small sphere particles existed on the surface of WO₃ plate. X-ray photoelectron spectroscopy (XPS) showed a higher concentration of Hf element than the result of energy-dispersive X-ray spectroscopy (EDX), which means that HfO₂ is rich on the surface of WO₃ plates. A higher photocurrent under visible light irradiation was gained with surface passivation. Meanwhile, the results of intensity modulated photocurrent spectrum (IMPS) and incident photon to current conversion efficiency (IPCE) indicate that HfO₂ passivation layer, acting as a barrier for the interfacial recombination, is responsible for the improved photoelectrochemical performance of WO₃ vertical plate-like arrays film.

Keywords: WO₃; HfO₂; surface passivation; photoelectrochemical performance

1. Introduction

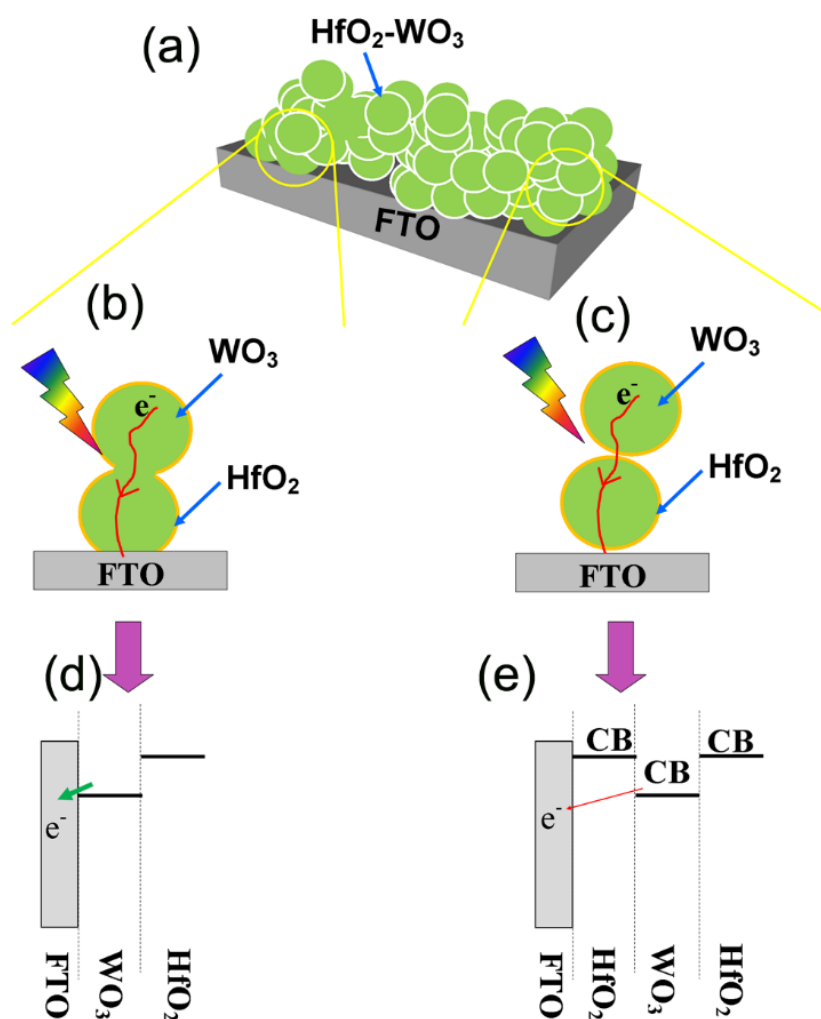
Photoelectrochemical (PEC) water splitting is a significant technology for relieving the energy crisis and environmental issues [1]. In the past decades, numerous researchers have focused on discovering novel solid-state catalysts that can effectively split water using either unbiased or externally biased electrodes. Since wide-band gap semiconductors like TiO_2 [2] and ZnO [3] were studied as photocatalysts for water-splitting, more recent efforts have turned to WO_3 due to its bandgap of 2.6 eV [4], its photostability in acidic conditions [5] and its good hole mobility [6].

Recently, WO_3 has been grown on the conductive substrate by hydrothermal technique, which has produced nanowire or nanoflake arrays by adjusting solution composition [7–9]. The WO_3 film with special oriented or one dominant facet was fabricated using different capping agents [10,11]. In other works, WO_3 vertical plate-like and rod-like array films have also been obtained by the hydrothermal method without seed layer [5,12]. The above vertically aligned films show satisfactory photoelectrochemical properties because two-dimensional arrays can provide a direct pathway for efficient charge transport. At the same time, co-catalysts like ZnO , BiVO_4 and TiO_2 were loaded on the WO_3 electrodes to improve photoelectrochemical performance [13–15]. In order to enhance catalytic performance, some strategies (doped with metal or nonmetal elements [16–18] and modified with noble metals [19,20]) have also been reported. Furthermore, surface passivation processes were introduced to PEC, with the aim of decreasing surface charge recombination. Alumina overlayer as a passivation layer loading on the WO_3 surface by atomic layer deposition, which reduced the number of electron trapping sites on the surface of WO_3 , eventually facilitated the photoelectron transfer to the external circuit in the presence of a positive bias [21].

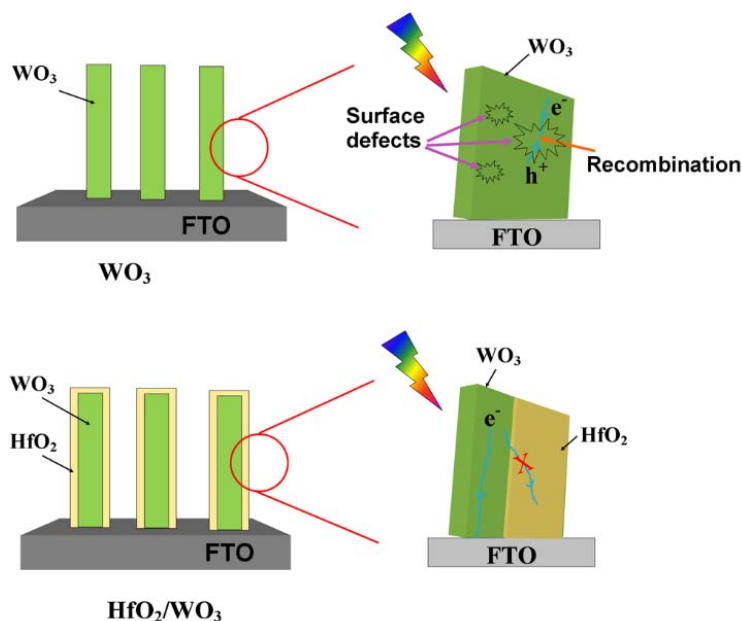
HfO_2 has been considered one of the most promising candidates of passivation layer in dye sensitized solar cells (DSSC) due to its wide band gap and chemical stability. Baroughi *et al.* found that the incorporation of HfO_2 layer resulted in a 69% improvement in the efficiency of the cell [22]. Kim *et al.* gained a similar result, and the lifetime of photoelectron increased after introducing hafnium oxide layer that could effectively retard the electron recombination process between nanocrystalline TiO_2 and electrolyte [23]. Ziegler *et al.* deposited HfO_2 or TiO_2 compact layer on the surfaces of ITO nanowires, and then coated porous TiO_2 layer. After coating of the compact layer, the efficiency of DSSC had been improved. Even though the wide band gap of HfO_2 was conducive to retarding the electron transfer from indium tin oxides (ITO) to electrolyte, the charge collection was also suppressed because the conduction band of HfO_2 is more negative than that of TiO_2 . The photocurrent of DSSC with HfO_2 compact layer was not as well as that with TiO_2 compact layer [24]. Hence, the high band gap materials (such as HfO_2) are not preferentially recommended to deposit between conductive substrate and photoresponse material.

In our previous paper [25], HfO_2 had been loaded on the surface of WO_3 nanoparticles, and then prepared into film as photoanodes. Despite the fact that HfO_2 has made progress in decreasing the surface defects of the WO_3 nanoparticles and improving the photoelectrochemical performance, an unwilling phenomenon occurs. Because the WO_3 particles were covered with HfO_2 before the film was prepared, and the charge transport in WO_3 nanoparticles film occurred via a random walk in a trap-limited diffusion process, a certain amount of photo-generated electrons transferred to fluorine-doped tin oxide (FTO) through HfO_2 layer, and the HfO_2 might have acted as a compact layer when it was inserted between the interfaces of FTO and WO_3 (Scheme 1). The more negative conduction band (CB) edge position of HfO_2 that forms an energy barrier would suppress electrons transport, similar to the

conclusion of Ziegler *et al.* [24]. Hence, a surficial passivation layer without the compact layer should exhibit better photoelectrochemical performance in theory. WO_3 vertical plate-like arrays provide a direct pathway for charge transport, and thus the electron transfer to FTO through the inner instead of surface of WO_3 plate. However, the surface recombination due to surface defects also hinders the performance improvement, and the surface passivation is still needed (Scheme 2). In addition, the particle size of HfO_2 and WO_3 nanoparticles might be similar, and it is hard for us to distinguish them from too low to distinguish from each other in the previous work. Thus, the obviously different size of HfO_2 and WO_3 plate provided a method to confirm and demonstrate the existence of surface passivation layer.



Scheme 1. Scheme of electron transport processes in the different section of photoanode. (a) WO_3 nanoparticle film coating of HfO_2 passivation layer; (b) photo-generated electrons transfer from WO_3 to FTO directly; (c) photo-generated electrons transfer from WO_3 to FTO through HfO_2 layer; (d) a structure of FTO/ WO_3 / HfO_2 ; and (e) a compact HfO_2 layer inserted between FTO and WO_3 . In the diagram, the arrows represent electron transfer from WO_3 to FTO, and the width of arrow represents the ability of electron transport.



Scheme 2. Scheme of the structures of WO_3 and HfO_2/WO_3 films. It is easy for the photo-generated electrons to recombine with photo-generated holes at the surface defect points of the WO_3 plates. With the passivation layer of HfO_2 , the surface defect points are covered so that the recombination is inhibited at the surface of WO_3 plates.

Herein, in this paper, we reported a dip-coating method to load HfO_2 on the surface of WO_3 vertical plate-like arrays. The HfO_2 could be clearly seen in the images of scanning electron microscopy and transmission electron microscopy, which verified that HfO_2 existed as overlayers on the surface of WO_3 plates. Meanwhile, the influence of HfO_2 passivation layer on the photoelectrochemical performance of WO_3 is studied elaborately using several methods.

2. Results and Discussion

2.1. Characterization of the As-Prepared Films

SEM and TEM were utilized to investigate the morphology and microstructure of samples. Typical SEM images of HfO_2/WO_3 and WO_3 are presented in Figure 1. In the top-views (Figure 1a,b), the low-magnification SEM images show that both samples exhibit plate-like structure with the plate thickness of 240–400 nm. The cross-sectional views (Figure 1c,d) show that the plate-like arrays grow perpendicular to the substrate, and the thickness of each film is about 1.16 μm . In other words, the structures are well retained after dip-coating and annealing. In the inset of Figure 1b, pure WO_3 presents a smooth surface. However, some spherical particles are tightly attached to the surface of HfO_2/WO_3 plates (inset of Figure 1a). Correspondingly, EDX spectra of the two samples were also recorded and shown in Figure 1e,f, which show that Hf exists in the HfO_2/WO_3 film. More details of size, shape and structural features can be analyzed from the TEM images (Figure 2). Figure 2a displays the plate-like structure of WO_3 film after the surface passivation process, and a fuzzy layer covers the surface of the plate. According to EDX analyses of the different parts, the nanoparticles at the edge of the plate (blue circle) is enriched with Hf relative to the bulk of the plate (red circle). It means that a layer of HfO_2 was

loaded on the surface of WO_3 plate. In Figure 2b, high-resolution transmission electron microscopy (HRTEM) image exhibits that the interplanar distance of the nanoparticle is about 0.283 nm, which is in agreement with the (111) crystal plane of HfO_2 . Therefore, we can verify that Hf exists as HfO_2 , which covers the surfaces of the WO_3 vertical plate-like arrays.

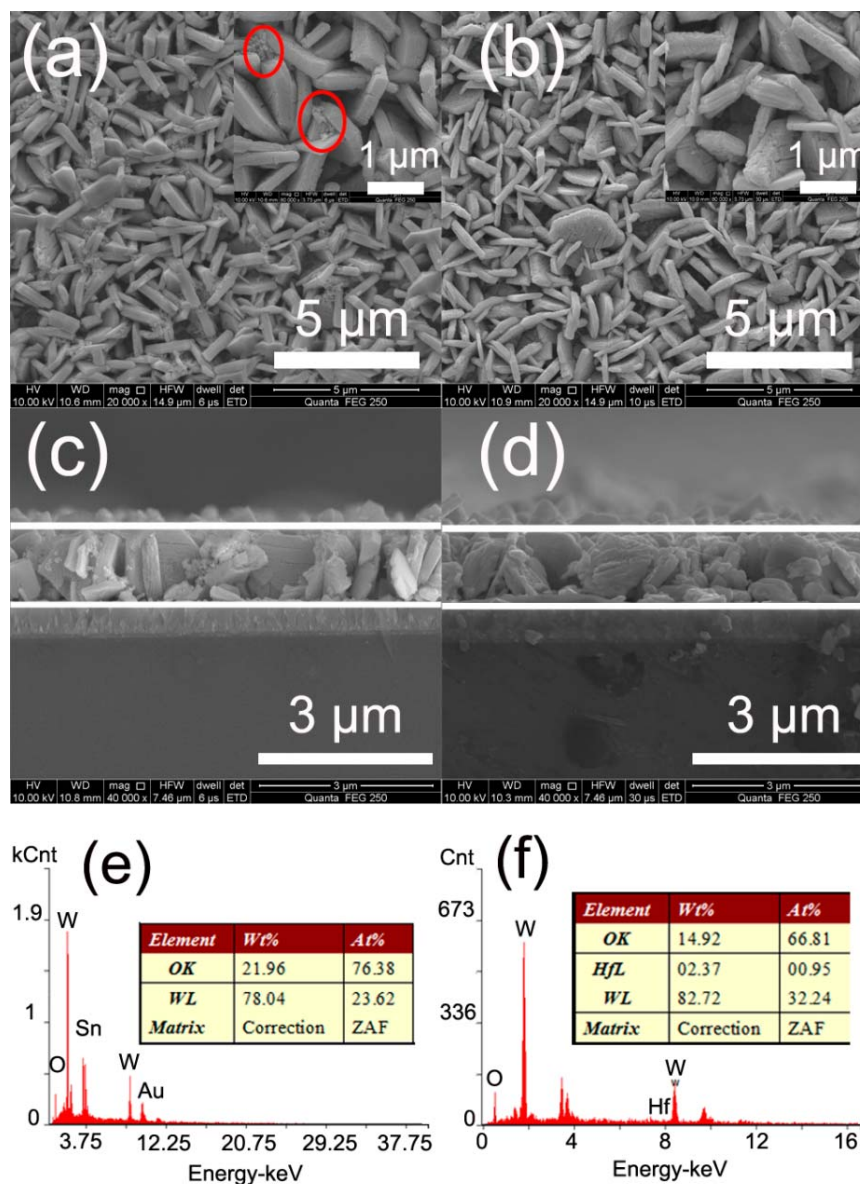


Figure 1. SEM images of the surface morphology of (a) HfO_2/WO_3 and (b) WO_3 ; cross-sectional micrographs of (c) HfO_2/WO_3 and (d) WO_3 ; high-magnification SEM images in inset of (a) and (b); and energy dispersive spectra of (e) WO_3 and (f) HfO_2/WO_3 film.

X-ray photoelectron spectroscopy (XPS) was employed to further confirm the surface composition and chemical states of WO_3 and HfO_2/WO_3 , as shown in Figure 3. Figure 3a presents low-resolution full range XPS spectra of both samples. The total XPS spectra indicate the presence of tungsten and oxygen, and hafnium element can also be seen in the spectrum of HfO_2/WO_3 . Meanwhile, the carbon peak (C1s) appearing at about 284 eV is due to adventitious carbon species from the XPS instrument. In Figure 3b, $\text{W}4f$ can be deconvoluted into a doublet with binding energy peaks at 35.70 eV and 37.85 eV,

resulting from the emission of W4f7/2 and W4f5/2 core-levels that might belong to the W⁶⁺ oxidation state of tungsten atoms [18]. For HfO₂/WO₃, the characteristic peaks of W⁶⁺ 4f_{7/2} and W 4f_{5/2} are shifted about 0.08 eV to a higher binding energy, indicating that some Hf atoms might have embedded into the WO₃ lattice. In Figure 3c, for WO₃, the peaks at 530.5 and 531.8 eV can be attributed to the lattice oxygen in WO₃ and OH group, respectively [26]. For HfO₂/WO₃, an additional peak at 530.7 eV is assigned to Hf-O band [27]. Figure 3d shows the Hf 4f spectrum of HfO₂/WO₃, and two peaks at 17.39 and 18.99 eV can be ascribed to Hf 4f_{7/2} and Hf 4f_{5/2} [28]. This indicates that the Hf element exists in the state of HfO₂. At the same time, the ratio of [Hf]/[W] = 0.28 has also been estimated, which is higher than the result of EDX (Figure 4c). Considering the detecting depth is different between EDX and XPS, it can be concluded that most of Hf atoms were enriched on the surface of WO₃ plates in the form of HfO₂, which is in line with the results of TEM in the Figure 2.

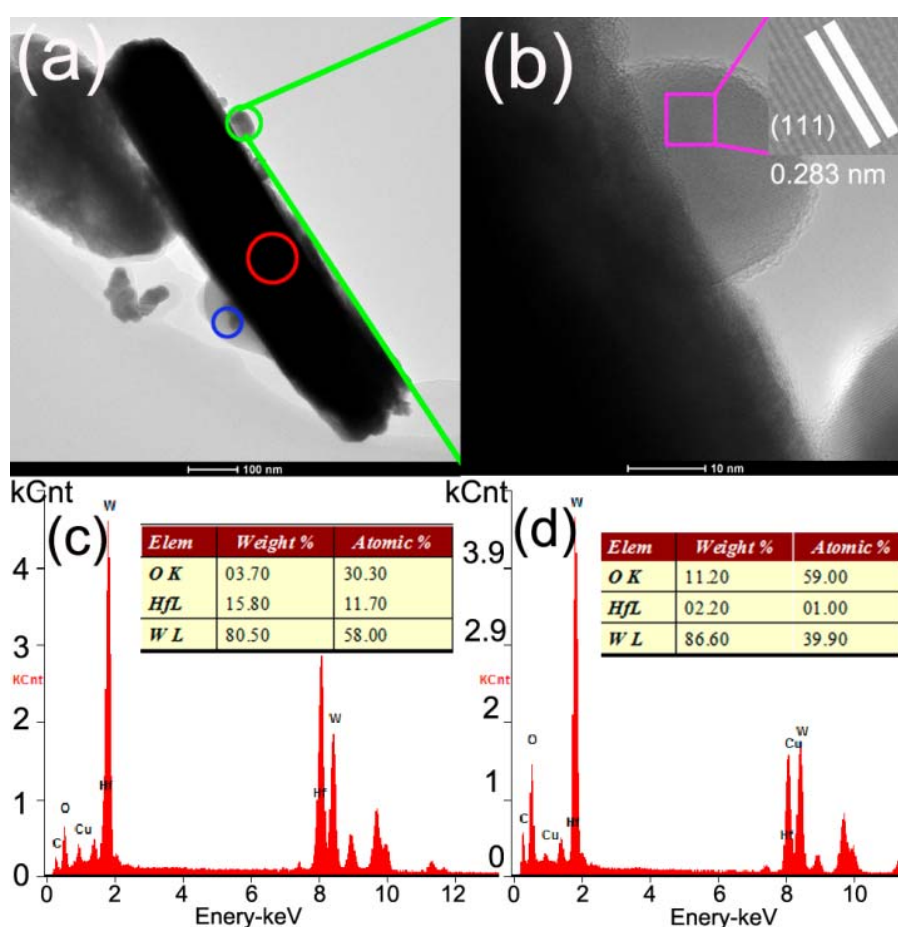


Figure 2. (a) Transmission electron micrographs and (b) high resolution TEM (HRTEM) image of WO₃ vertical plate-like film after the surface passivation; and EDX spectra corresponding to different sections in the inset of (a): (c) blue circle and (d) red circle.

The corresponding XRD patterns in Figure 4 indicate that both of the samples match well with the monocline WO₃ (PDF#72-0677). Moreover, the peaks at 37.77°, 51.76° and 65.74° belong to the (200), (211) and (301) facets of the tetragonal structure of SnO₂ (PDF#46-1088), indicating that the samples are loaded on the FTO. The peaks corresponding to HfO₂ cannot be found, which is originated from two reasons. One is that the concentration of HfO₂ is less than the detection limit of XRD. The other is that

the HfO₂ in the sample are dispersed on the surface of WO₃ nanoplates uniformly and sparsely, which has been confirmed by TEM.

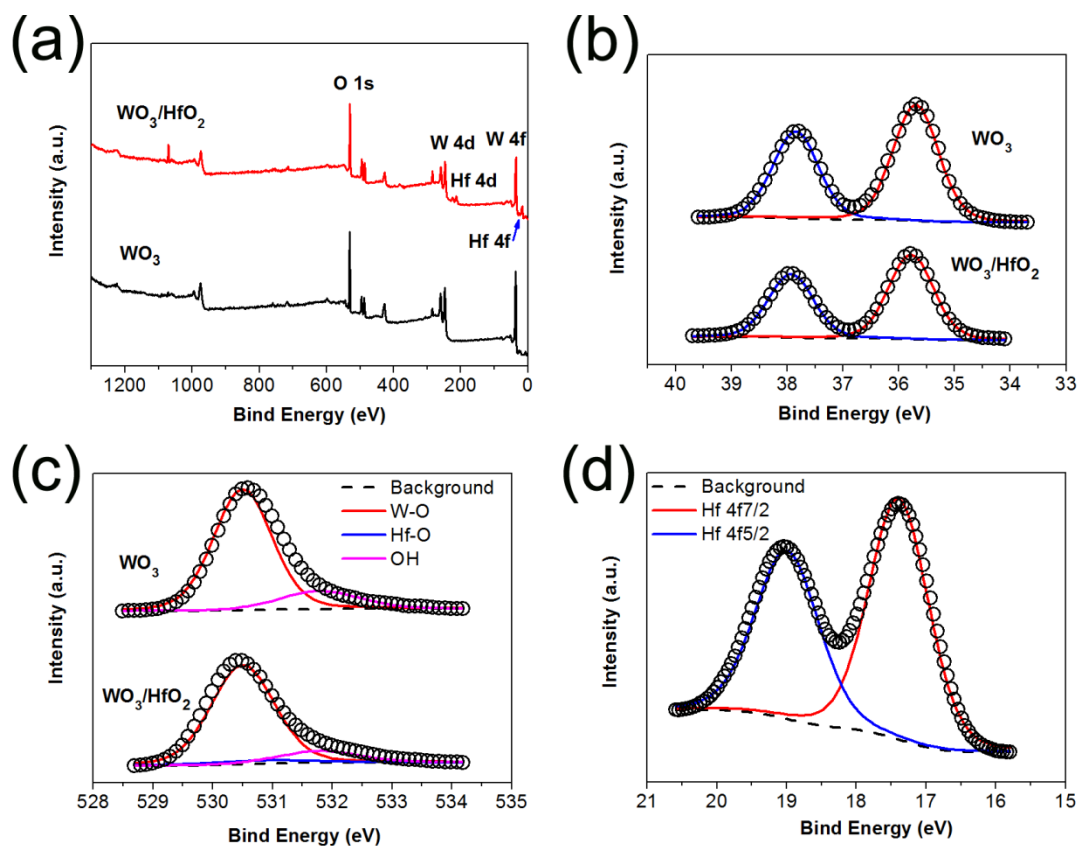


Figure 3. X-ray photoelectron spectroscopy (XPS) spectra of the WO₃ and HfO₂/WO₃ films: (a) the full spectrum, (b) W 4f spectrum, (c) O 1s, and (d) Hf 4f.

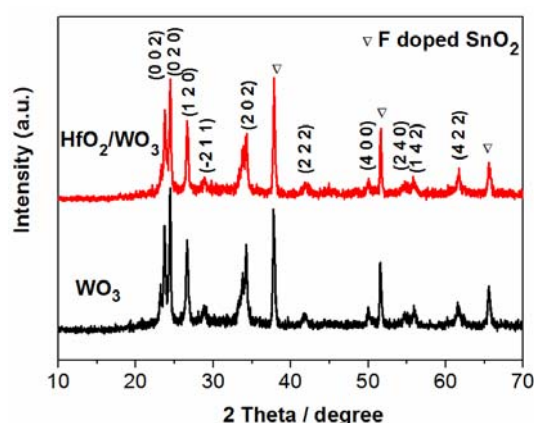


Figure 4. X-ray diffraction (XRD) patterns of WO₃ and HfO₂/WO₃.

The light-absorbance properties of WO₃ vertical plate-like film before and after the surface passivation were probed with UV-vis diffuse reflectance spectroscopy, as shown in Figure 5. Compared with WO₃, a broad background absorption in the visible light region is observed after the surface passivation, which is similar to Kim's work [23]. It can be ascribed to the fact that the surface of WO₃ plate has been changed after the loading of HfO₂. The absorption edge of HfO₂/WO₃ has no obvious shift compared

with WO_3 , and it is 470 and 473 nm for WO_3 and HfO_2/WO_3 , respectively. Correspondingly, the band gap of WO_3 and HfO_2/WO_3 is 2.64 and 2.62 eV, respectively, which is estimated using the following equations [18]:

$$\alpha h\nu = A(h\nu - E_g)^n \quad (1)$$

The slight difference of band gap between two samples is because that several Hf atoms are embedded in the WO_3 lattice, which is consistent with the result of DFT calculation in the work of Valentin *et al* [29].

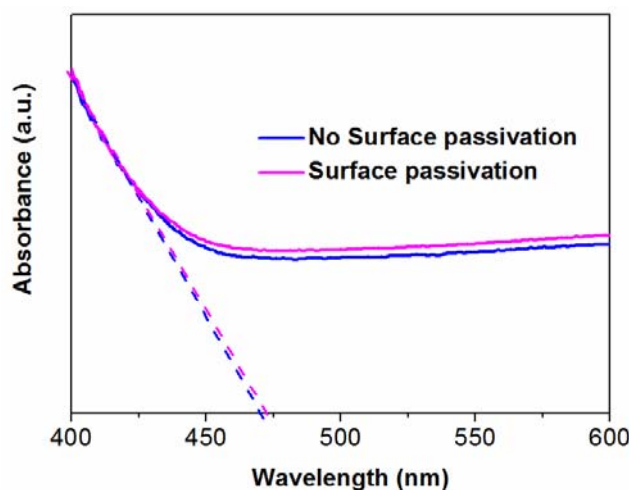


Figure 5. UV-vis absorbance spectra of WO_3 vertical plate-like film with and without the surface passivation layer.

2.2. Photoelectrochemical Measurements of the Films

Figure 6a shows linear sweep voltammetry measurements to determine the photocurrent densities of WO_3 and HfO_2/WO_3 photoanodes. The photocurrent density of WO_3 increases gradually with the increase of applied potential. After loading of HfO_2 , the photocurrent is enhanced compared to the pristine WO_3 , which is similar to the alumina/ Fe_2O_3 films [30]. The photocurrent values of WO_3 and HfO_2/WO_3 at 1.0 V (*vs.* Ag/AgCl) are about 0.75 and 0.90 mA/cm^2 , respectively. The stability of WO_3 and HfO_2/WO_3 were also investigated and measured at 1.0 V (*vs.* Ag/AgCl). In Figure 6b, the photocurrent value rapidly decreases to about zero as soon as the light is chopped. It means that there is no other reaction occurred under dark condition. At the same time, the photocurrent values of WO_3 and HfO_2/WO_3 decrease 29.0% (from 0.81 to 0.57 mA/cm^2) and 24.4% (from 0.94 to 0.71 mA/cm^2), respectively, after irradiation of 1180 s. This indicates that the HfO_2/WO_3 film shows better stability compared to the bare WO_3 film. The photoelectrochemical performances of both photoanodes are also estimated by the light energy to chemical energy efficiency, which is calculated with the following equation [31,32].

$$\varepsilon(\%) = j_i \{ (E_{re}^\circ - |E_{app}|) \} / I_o \times 100 \quad (2)$$

In this equation, j_i , E_{re}° , E_{app} and I_o are the photocurrent density, the standard reversible potential, the applied potential of the working electrode and power density of the incident light, respectively. As illustrated in Figure 6c, the maximum photoconversion efficiency of HfO_2/WO_3 (0.30%) is greater than that of WO_3 (0.25%).

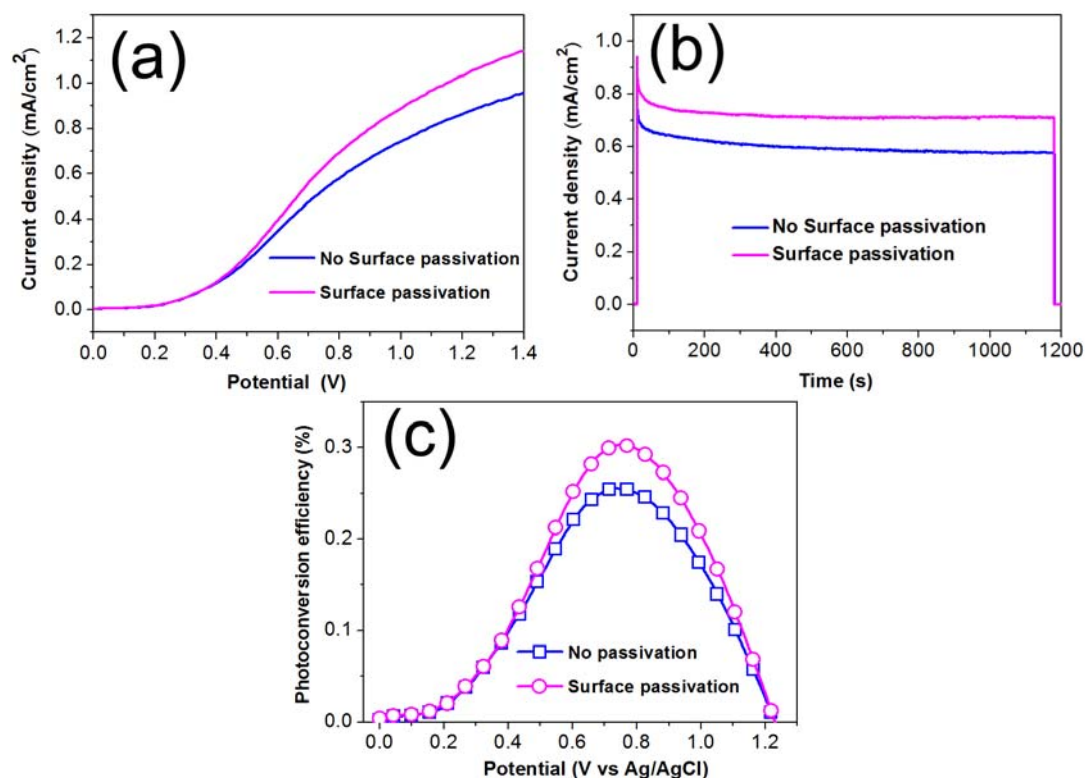


Figure 6. (a) Linear sweep voltammetry curves of WO₃ vertical plate-like film with and without the surface passivation layer under light illumination; (b) photocurrent-time plot of the samples under illumination; and (c) Photoconversion efficiency of the as-prepared samples.

Electrochemical impedance spectroscopy (EIS) analysis has been regarded as a useful tool for investigating the kinetics of photoelectrochemical processes. To better understand the dynamics of electron transport and reveal the difference in the interfacial characteristics of the WO₃ vertical plate-like film with and without the surface passivation layer, the EIS of photoelectrodes were measured, as shown in Figure 7. In each Nyquist plot (Figure 7a), the semicircle denotes the charge transfer at the photoanode/electrolyte interface, which can be fitted by using an equivalent circuit containing a series resistance (R_s), a charge transfer resistance (R_{ct}) and a constant phase element (CPE) (inset of Figure 7a). The results of the EIS analysis show that a smaller value of R_{ct} is seen for HfO₂/WO₃ (433.2 ohm) compared with WO₃ (584.2 ohm), which implies that HfO₂ layer promotes more efficient charge transfer at the photoanode/electrolyte interface. The bode phase plots of EIS spectra (Figure 7b) display the frequency peaks of the charge transfer process at the interface of each photoanode. The maximum oscillation frequency (f_{max}) of the impedance semicircle of HfO₂/WO₃ is less than that of WO₃. Considering electron lifetime (τ_e) is inversely proportional to f_{max} , the corresponding lifetime of photoelectrons in HfO₂/WO₃ increases compared to WO₃. According to the equation [33]:

$$\tau_e = 1/2\pi f_{max} \quad (3)$$

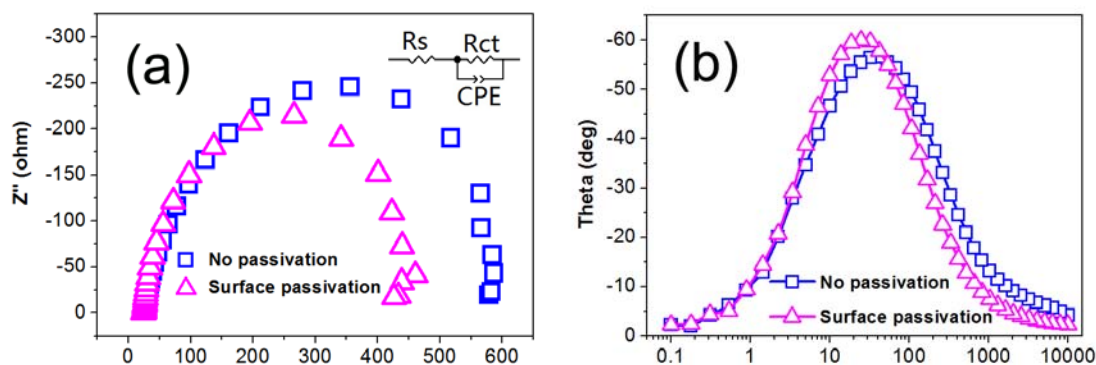


Figure 7. EIS plots of the WO_3 vertical plate-like film before and after the surface passivation: (a) Nyquist plots and (b) Bode plots; equivalent circuit in the inset of (a).

The values of τ_e are 3.8 and 6.5 ms for WO_3 and HfO_2/WO_3 , respectively. The above discussion indicates that HfO_2 coverage acts as a barrier for the recombination of photo-generated electrons and holes at the photoanode/electrolyte interface, decreasing the recombination rate of electron-hole pairs. Moreover, the CB of HfO_2 is less than that of WO_3 , the HfO_2 layer on the surface of WO_3 plates as an electron-blocking layer may hinder the photo-generated electrons from transferring to the interface of photoanode/electrolyte. The effect might be non-significant because the plate-like arrays with good charge transport ability and positive bias for photoanode have good effect on transferring the photoelectrons to FTO and external circuit. Furthermore, the valence band of HfO_2 (3.0–3.2 eV) [34,35] is slightly less than that of WO_3 (3.0–3.35 eV) [36,37]. It is hard to say that the small difference of valence band has obvious effect on the transferring hole from WO_3 to HfO_2 , but we believe that the negative effect would not occur in this system. Anyhow, these facilitate the charge transfer efficiently so as to enhance the photoelectrochemical performance.

Intensity modulated photocurrent spectrum (IMPS) data were recorded and used to investigate electron transport. Figure 8 shows the complex plane plots of the IMPS responses for both samples. The response appears in the fourth quadrant of the complex plane and displays one semicircle, where the frequency at the imaginary minimum of the semicircle can be used to calculate the time constant of the charge transfer process. The electron transport time (τ_{tr}) can be estimated from the equation [14]:

$$\tau_{tr} = 1/(2\pi f_{(IMPS)}) \quad (4)$$

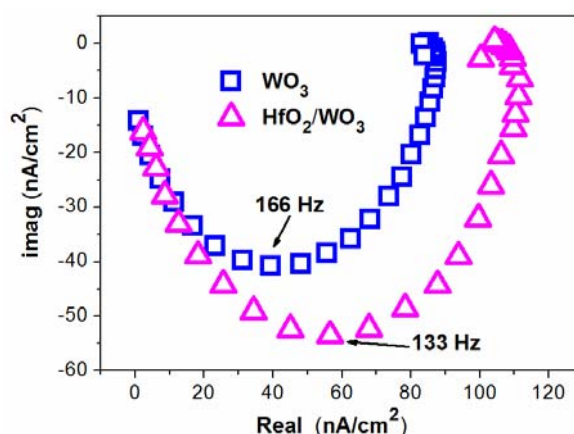


Figure 8. Intensity-modulated photocurrent spectroscopies of WO_3 and HfO_2/WO_3 .

The electron transport times calculated for WO_3 and HfO_2/WO_3 are 0.96 and 1.20 ms, respectively. The longer electron transport time might be caused by some Hf atoms occupying into the WO_3 lattice, which affect the crystallinity of WO_3 plates so that the charge transport ability of HfO_2/WO_3 is not as good as that of WO_3 . Even though a long transport time provides no benefit to the photoelectrochemical properties, the photocurrent of HfO_2/WO_3 is still higher than that of WO_3 . Hence, the passivation layer, which acts as a barrier for the interfacial recombination, is the main reason of the improved photoelectrochemical performance.

Incident photon-to current efficiency (IPCE), which reflects the number of electrons in the external circuit produced by an incident photon at a given wavelength divided by the number of incident photons, is an effective tool to investigate the quantitative correlation of light absorption on the WO_3 vertical plate-like film with and without the surface passivation layer. Figure 9 shows the plots of both samples at a bias of 1.0 V. The HfO_2/WO_3 exhibits a higher IPCE value compared to WO_3 , in agreement with the results of linear sweep photovoltammetry measurements (Figure 6a). Both samples display a strong photon response in the region of 310–460 nm, and the maximum values are 30.92% and 36.54% for WO_3 and HfO_2/WO_3 , respectively. Based on the above results and the enhancement of IPCE existing in the whole photoresponse region, we can conclude that the HfO_2 passivation layer, which inhibits the recombination of electrons and holes, is the major reason for enhancing photoelectrochemical performance of WO_3 vertical plate-like arrays.

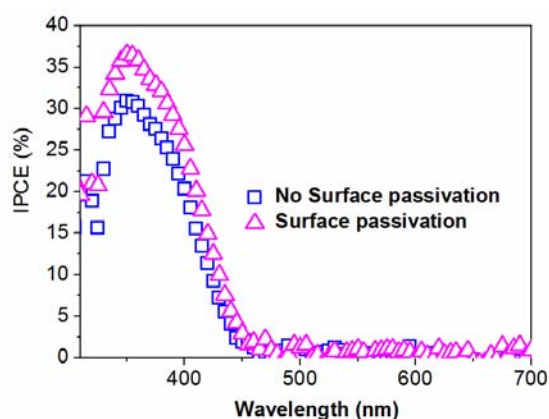


Figure 9. Incident photo to current conversion efficiency of WO_3 vertical plate-like film with and without the surface passivation layer.

3. Experimental Section

3.1. Sample Preparation

All chemicals were analytical grade and used without further purification. WO_3 vertical array film was fabricated via a facile hydrothermal method [38]. To synthesize the WO_3 vertical array film with a HfO_2 surface passivation layer (HfO_2/WO_3), as-prepared WO_3 film was immersed in a 40 mL concentrated sulfuric acid solution that 30 mg HfO_2 had been dissolved in. After dipping of 2 min, the substrate with WO_3 film was taken out and immersed in deionized water immediately. Then, the film was dried naturally, and the two-step dipping procedure was repeated again. Finally, the prepared sample was

obtained after being dried in an oven at 60 °C and annealed at 450 °C for 30 min. For comparison, the bare WO₃ film was also treated in a similar method without the addition of HfO₂.

3.2. Structure Characterization

The structure and morphology of prepared samples were characterized with a field emission scanning electron microscope (FESEM, JSM-7600F, JEOL Company, Tokyo, Japan) and a transmission electron microscope (TEM, TECNAI G2 F20, FEI, Japan) equipped with an energy-dispersive X-ray (EDX) spectrometer. The crystal phases were identified by X-ray diffraction (XRD, D/Max2250, Rigaku Corporation, Japan) with Cu K α radiation. X-ray photoelectron spectroscopy (XPS, ESCALAB 250Xi, Thermo Fisher-VG Scientific) was used to determine the chemical composition and the concentration of the atoms. UV-visible (UV-vis) absorption spectra in the range of 400–600 nm were detected by a diffused reflectance ultraviolet and visible spectrophotometer (UV-vis, PGeneral TU-1901, Beijing, China).

3.3. Photoelectrochemical Measurements

A standard three-electrode system was used to evaluate the photoelectrochemical properties with an electrochemical analyzer (Zennium, Zahner, Germany). The sample served as the photoanode, a Pt foil as the counter electrode and an Ag/AgCl (saturated KCl) as the reference electrode. An aqueous solution of 0.2 M Na₂SO₄ was used as the electrolyte solution. Linear sweep voltammetry were measured in a potential range from 0 V to 1.4 V (*vs.* Ag/AgCl) under AM 1.5G illumination. The electrochemical impedance spectra (EIS) were measured at 0.7 V (*vs.* Ag/AgCl) with perturbation amplitude of 10 mV, frequency of 0.1 Hz~10 kHz. Mott-Schottky plots were monitored at the AC frequency of 1 kHz, and the potential ranged from 0 to 1.0 V. Intensity modulated photocurrent spectrum (IMPS) data were recorded using a Zahner CIMPS-2 system (Zahner CIMPS-2, Zahner, Germany). Meanwhile, the incident photon to current conversion efficiency (IPCE) was carried out as a function of wavelength from 310 to 700 nm with Si solar cell as standard.

4. Conclusions

In summary, we report a simple dip-coating and annealing method to synthesize HfO₂ passivation layer loaded on the surface of WO₃ vertical plate-like arrays. The differences in morphology between WO₃ and HfO₂/WO₃ can be clearly seen in the SEM and TEM measurements, and the HfO₂ nanoparticles can be distinguished from the WO₃ plates due to different sizes and interplanar distances. The different concentrations of Hf detected by EDX and XPS indicate that HfO₂ is rich on the surface of WO₃ plates. HfO₂/WO₃ photoanode exhibits a higher photocurrent under visible light irradiation compared to WO₃ photoanode. At the same time, the electron transport time has been slightly increased, which suggests charge transport ability has not been modified. Hence, the improvement of IPCE confirms that HfO₂ passivation layer, acting as a barrier for the interfacial recombination, is in favor of the improvement the photoelectrochemical performance of WO₃ vertical plate-like arrays film.

Acknowledgments

This study was supported by the National High Technology Research and Development Program of China (2011AA050528), the National Natural Science Foundation of China (21171175) and Postgraduate research and innovation project of Hunan Province (cx2015b266).

Author Contributions

Jie Li, Wenzhang Li and Yang Liu contributed to the experimental design; Yang Liu and Renrui Xie contributed to all the experimental data collection; Yahui Yang and Yang Liu wrote the paper.

Conflicts of Interest

The authors declare no conflict of interest.

References

1. Kapilashrami, M.; Zhang, Y.; Liu, Y.-S.; Hagfeldt, A.; Guo, J. Probing the Optical Property and Electronic Structure of TiO₂ Nanomaterials for Renewable Energy Applications. *Chem. Rev.* **2014**, *114*, 9662–9707.
2. Wang, G.; Wang, H.; Ling, Y.; Tang, Y.; Yang, X.; Fitzmorris, R.C.; Wang, C.; Zhang, J.Z.; Li, Y. Hydrogen-treated TiO₂ nanowire arrays for photoelectrochemical water splitting. *Nano Lett.* **2011**, *11*, 3026–3033.
3. Kargar, A.; Jing, Y.; Kim, S.J.; Riley, C.T.; Pan, X.; Wang, D. ZnO/CuO Heterojunction Branched Nanowires for Photoelectrochemical Hydrogen Generation. *ACS Nano* **2013**, *7*, 11112–11120.
4. Amano, F.; Tian, M.; Wu, G.; Ohtani, B.; Chen, A. Facile preparation of platelike tungsten oxide thin film electrodes with high photoelectrode activity. *ACS Appl. Mater. Interfaces* **2011**, *3*, 4047–4052.
5. Kalanur, S.S.; Hwang, Y.J.; Chae, S.Y.; Joo, O.S. Facile growth of aligned WO₃ nanorods on FTO substrate for enhanced photoanodic water oxidation activity. *J. Mater. Chem. A* **2013**, *1*, 3479–3488.
6. Zheng, J.Y.; Haider, Z.; Van, T.K.; Pawar, A.U.; Kang, M.J.; Kim, C.W.; Kang, Y.S. Tuning of the crystal engineering and photoelectrochemical properties of crystalline tungsten oxide for optoelectronic device applications. *CrystEngComm* **2015**, *17*, 6070–6093.
7. Su, J.; Feng, X.; Sloppy, J.D.; Guo, L.; Grimes, C.A. Vertically aligned WO₃ nanowire arrays grown directly on transparent conducting oxide coated glass: Synthesis and photoelectrochemical properties. *Nano Lett.* **2010**, *11*, 203–208.
8. Amano, F.; Tian, M.; Ohtani, B.; Chen, A. Photoelectrochemical properties of tungsten trioxide thin film electrodes prepared from facet-controlled rectangular platelets. *J. Solid State Electrochem.* **2012**, *16*, 1965–1973.
9. Amano, F.; Li, D.; Ohtani, B. Photoelectrochemical property of tungsten oxide films of vertically aligned flakes for visible-light-induced water oxidation. *J. Electrochem. Soc.* **2011**, *158*, K42–K46.
10. Zheng, J.Y.; Song, G.; Kim, C.W.; Kang, Y.S. Fabrication of (001)-oriented monoclinic WO₃ film on FTO substrate. *Nanoscale* **2013**, *5*, 5279–5282.

11. Zheng, J.Y.; Song, G.; Hong, J.; Van, T.K.; Pawar, A.U.; Kim, D.Y.; Kim, C.W.; Haider, Z.; Kang, Y.S. Facile Fabrication of WO₃ Nanoplates Thin Films with Dominant Crystal Facet of (002) for Water Splitting. *Cryst. Growth Des.* **2014**, *14*, 6057–6066.
12. Yang, J.; Li, W.; Li, J.; Sun, D.; Chen, Q. Hydrothermal synthesis and photoelectrochemical properties of vertically aligned tungsten trioxide (hydrate) plate-like arrays fabricated directly on FTO substrates. *J. Mater. Chem.* **2012**, *22*, 17744–17752.
13. Liu, Y.; He, H.; Li, J.; Li, W.; Yang, Y.; Li, Y.; Chen, Q. ZnO nanoparticle-functionalized WO₃ plates with enhanced photoelectrochemical properties. *RSC Adv.* **2015**, *5*, 46928–46934.
14. Su, J.; Guo, L.; Bao, N.; Grimes, C.A. Nanostructured WO₃/BiVO₄ Heterojunction Films for Efficient Photoelectrochemical Water Splitting. *Nano Lett.* **2011**, *11*, 1928–1933.
15. Szilágyi, I.M.; Santala, E.; Heikkilä, M.; Pore, V.; Kemell, M.; Nikitin, T.; Teucher, G.; Firkala, T.; Khriachtchev, L.; Räsänen, M.; Ritala, M.; Leskelä, M. Photocatalytic Properties of WO₃/TiO₂ Core/Shell Nanofibers prepared by Electrospinning and Atomic Layer Deposition. *Chem. Vap. Depos.* **2013**, doi:10.1002/cvde.201207037.
16. Sun, Y.; Murphy, C.J.; Reyes-Gil, K.R.; Reyes-Garcia, E.A.; Thornton, J.M.; Morris, N.A.; Raftery, D. Photoelectrochemical and structural characterization of carbon-doped WO₃ films prepared via spray pyrolysis. *Int. J. Hydrogen Energy* **2009**, *34*, 8476–8484.
17. Liu, Y.; Li, J.; Li, W.; Yang, Y.; Li, Y.; Chen, Q. Enhancement of the Photoelectrochemical Performance of WO₃ Vertical Arrays Film for Solar Water Splitting by Gadolinium Doping. *J. Phys. Chem. C* **2015**, *119*, 14834–14842.
18. Zhang, T.; Zhu, Z.; Chen, H.; Bai, Y.; Xiao, S.; Zheng, X.; Xue, Q.; Yang, S. Iron-doping-enhanced photoelectrochemical water splitting performance of nanostructured WO₃: A combined experimental and theoretical study. *Nanoscale* **2015**, *7*, 2933–2940.
19. Xu, F.; Yao, Y.; Bai, D.; Xu, R.; Mei, J.; Wu, D.; Gao, Z.; Jiang, K. Au nanoparticle decorated WO₃ photoelectrode for enhanced photoelectrochemical properties. *RSC Adv.* **2015**, *5*, 60339–60344.
20. Ghosh, S.; Acharyya, S.S.; Kumar, M.; Bal, R. One-pot preparation of nanocrystalline Ag-WO₃ catalyst for the selective oxidation of styrene. *RSC Adv.* **2015**, *5*, 37610–37616.
21. Kim, W.; Tachikawa, T.; Monllor-Satoca, D.; Kim, H.-I.; Majima, T.; Choi, W. Promoting water photooxidation on transparent WO₃ thin films using an alumina overlayer. *Energy Environ. Sci.* **2013**, *6*, 3732–3739.
22. Shanmugam, M.; Baroughi, M.F.; Galipeau, D. Effect of atomic layer deposited ultra thin HfO₂ and Al₂O₃ interfacial layers on the performance of dye sensitized solar cells. *Thin Solid Films* **2010**, *518*, 2678–2682.
23. Ramasamy, P.; Kang, M.-S.; Cha, H.-J.; Kim, J. Highly efficient dye-sensitized solar cells based on HfO₂ modified TiO₂ electrodes. *Mater. Res. Bull.* **2013**, *48*, 79–83.
24. Li, L.; Xu, C.; Zhao, Y.; Chen, S.; Ziegler, K.J. Improving Performance via Blocking Layers in Dye-Sensitized Solar Cells Based on Nanowire Photoanodes. *ACS. Appl. Mater. Interfaces* **2015**, *7*, 12824–12831.
25. Liu, Y.; Li, J.; Li, W.; Liu, Q.; Yang, Y.; Li, Y.; Chen, Q. Enhanced photoelectrochemical performance of WO₃ film with HfO₂ passivation layer. *Int. J. Hydrogen Energy* **2015**, *40*, 8856–8863.

26. Rettie, A.J.E.; Klavetter, K.C.; Lin, J.-F.; Dolocan, A.; Celio, H.; Ishiekwene, A.; Bolton, H.L.; Pearson, K.N.; Hahn, N.T.; Mullins, C.B. Improved Visible Light Harvesting of WO₃ by Incorporation of Sulfur or Iodine: A Tale of Two Impurities. *Chem. Mater.* **2014**, *26*, 1670–1677.
27. Cabello, G.; Lillo, L.; Buono-Core, G.E. Zr(IV) and Hf(IV) β -diketonate complexes as precursors for the photochemical deposition of ZrO₂ and HfO₂ thin films. *J. Non-Cryst. Solids* **2008**, *354*, 982–988.
28. Čížek, J.; Melikhova, O.; Procházka, I. Hydrogen-induced defects and multiplication of dislocations in Palladium. *J. Alloys Compd.* **2015**, *645*, S312–S315.
29. Wang, F.; di Valentin, C.; Pacchioni, G. Rational Band Gap Engineering of WO₃ Photocatalyst for Visible light Water Splitting. *ChemCatChem* **2012**, *4*, 476–478.
30. Le Formal, F.; Tetreault, N.; Cornuz, M.; Moehl, T.; Gratzel, M.; Sivula, K. Passivating surface states on water splitting hematite photoanodes with alumina overlayers. *Chem. Sci.* **2011**, *2*, 737–743.
31. Hsiao, P.-T.; Chen, L.-C.; Li, T.-L.; Teng, H. Vapor treatment of nanocrystalline WO₃ photoanodes for enhanced photoelectrochemical performance in the decomposition of water. *J. Mater. Chem.* **2011**, *21*, 19402–19409.
32. Devadoss, A.; Sudhagar, P.; Ravidhas, C.; Hishinuma, R.; Terashima, C.; Nakata, K.; Kondo, T.; Shitanda, I.; Yuasa, M.; Fujishima, A. Simultaneous glucose sensing and biohydrogen evolution from direct photoelectrocatalytic glucose oxidation on robust Cu₂O-TiO₂ electrodes. *Phys. Chem. Chem. Phys.* **2014**, *16*, 21237–21242.
33. Chen, K.; Feng, X.; Hu, R.; Li, Y.; Xie, K.; Li, Y.; Gu, H. Effect of Ag nanoparticle size on the photoelectrochemical properties of Ag decorated TiO₂ nanotube arrays. *J. Alloys Compd.* **2013**, *554*, 72–79.
34. Afanas'ev, V. V.; Stesmans, A.; Delabie, A.; Bellenger, F.; Houssa, M.; Meuris, M. Electronic structure of GeO₂-passivated interfaces of (100) Ge with Al₂O₃ and HfO₂. *Appl. Phys. Lett.* **2008**, *92*, 2109.
35. Rumaiz, A.K.; Woicik, J.C.; Carini, G.A.; Siddons, D.P.; Cockayne, E.; Huey, E.; Lysaght, P.S.; Fischer, D.A.; Genova, V. Band alignment of atomic layer deposited HfO₂ on clean and N passivated germanium surfaces. *Appl. Phys. Lett.* **2010**, *97*, 242108.
36. He, T.; Ma, Y.; Cao, Y.; Hu, X.; Liu, H.; Zhang, G.; Yang, W.; Yao, J. Photochromism of WO₃ Colloids Combined with TiO₂ Nanoparticles. *J. Phys. Chem. B* **2002**, *106*, 12670–12676.
37. Arai, T.; Yanagida, M.; Konishi, Y.; Iwasaki, Y.; Sugihara, H.; Sayama, K. Efficient Complete Oxidation of Acetaldehyde into CO₂ over CuBi₂O₄/WO₃ Composite Photocatalyst under Visible and UV Light Irradiation. *J. Phys. Chem. C* **2007**, *111*, 7574–7577.
38. Liu, C.; Yang, Y.; Li, W.; Li, J.; Li, Y.; Shi, Q.; Chen, Q. Highly Efficient Photoelectrochemical Hydrogen Generation Using Zn_xBi₂S_{3+x} Sensitized Platelike WO₃ Photoelectrodes. *ACS. Appl. Mater. Interfaces* **2015**, *7*, 10763–10770.